ELSEVIER

Ceramics International 28 (2002) 479–486

CERAMICS INTERNATIONAL

www.elsevier.com/locate/ceramint

Kinetics of the reactive sintering of kaolinite-aluminum hydroxide extrudate

Ya-Fei Liu[a], Xing-Qin Liu[a], Shan-Wen Tao[b], Guang-Yao Meng[a,*], O. Toff Sorensen[b]

[a]*Department of Materials Science and Engineering, University of Science and Technology of China, Anhui 230026, PR China*
[b]*The Center of Advanced Materials, The Riso National Laboratory, Denmark*

Received 24 May 2000; received in revised form 3 July 2000; accepted 3 October 2001

Abstract

The kinetics of the reactive sintering process of the extrudate made of a kaolinite and aluminum hydroxide mixture is investigated by means of stepwise isothermal dilatometry (SID) accompanied with XRD, SEM and other techniques. We find that the process can be divided into three stages in total, and the isothermal shrinkage data can be well-fitted according to Makipirtti–Meng equation: $dY/dt = nk(T)Y(1-Y)[(1-Y)/Y]^{1/n}$, where Y is the fractional densification function. The apparent activation energy E_a values are obtained as 2972 ± 461 kJ mol^{-1} for 950–1100 °C, 1056 ± 74 kJ mol^{-1} for 1200–1300 °C, and 792.7 ± 17.0 kJ mol^{-1} for 1300–1450 °C. The sintering shrinkage mechanisms in different temperature ranges are discussed, with reference to phase, pore and microstructure development. This study is helpful to control the microstructure and properties of the porous mullite-corundum ceramics.

Keywords: D. Al_2O_3; Kinetics; Kaolinite; Stepwise isothermal dilatometry; Porous mullite-corundum ceramics

1. Introduction

Mullite is the only stable crystalline aluminosilicate phase in the SiO_2–Al_2O_3 binary system. The ceramic materials based on it have a unique combination of excellent properties such as low density, good high-temperature strength and creep resistance, low thermal expansion coefficient and thermal conductivity, low dielectric constant, chemical inertness and thermal stability, and infrared transparency. All of these make mullite envisage promising application as advanced electrical, optical and structural ceramics [1–4].

The productions of high purity mullite by means of wet chemical routes are usually rather costly, which can only result in a small processing capacity product. Using the natural clay such as kaolinite as a starting material seems a cheaper option, but a high volume fraction of glassy phase appears due to the release of silica during heating as well as the impurities [5]. The troublesome glassy phase content might be reduced by adding an aluminous substance to kaolinite so as to produce secondary mullite in addition to primary mullite derived directly from kaolinite.

The preparations of mullite ceramics from kaolinite was previously reported by others [5–9]. However, little is known about the kinetics of their reactive sintering processes. For a composite material such as mullite-corundum ceramics, the sintering study is of momentous current significance for the direction of practical production. Thus, in the present work, we try to make an investigation into these composite ceramics.

2. A survey on the kinetic study of mullite formation

The methods used to study mullitization kinetics were generally based on dynamic X-ray diffraction (DXRD) [10–12], non-isothermal DTA [13], time resolved energy-dispersive powder diffraction [14] and differential scanning calorimetry (DSC) [15]. The kinetic models with specific experiential expression which have been used are usually as follows:

(a) the nucleation and growth model by Avrami [16]:

$$x = 1 - \exp(-k_A t^n) \quad (1)$$

* Corresponding author. Tel.: +86-551-3603234; fax: +86-551-3631760.
E-mail address: mgym@ustc.edu.cn (G.-Y. Meng).

0272-8842/02/$22.00
PII: S0272-8842(01)00120-1

where x is the volume fraction of crystallized mullite, k_A the rate constant, t the time, and n the time exponent;

(b) Johnson and Mehl model [17]:

$$x = 1 - (1 + K)\exp\left(\dot{N}\, t\right) \tag{2}$$

where K is a correction factor, $\dot{N}$ is the nucleation rate,

$$\dot{N} = A\exp\left(-\frac{\Delta G_{\mathrm{N}} + \Delta G_{\mathrm{D}}}{kT}\right) \tag{3}$$

where ΔG_{N} and ΔG_{D} are the activation energies for nucleus formation and diffusion across the phase boundary, respectively;

(c) The bimodel Johnson–Mehl–Avrami (JMA) model [15]:

$$\frac{\mathrm{d}x}{\mathrm{d}t} = A.\left\{\left[k_1^{n_1} n_1 (t-\tau_1)^{(n_1-1)}\right].\exp\left[-k_1^{n_1}(t-\tau_1)^{n_1}\right]\right\} + (1-A)\left\{\left[k_2^{n_2} n_2 (t-\tau_2)^{(n_2-1)}\right].\exp\left[-k_2^{n_2}(t-\tau_2)^{n_2}\right]\right\} \tag{4}$$

where x is the volume fraction of crystallized mullite, A is the ratio between enthalpy release attributed to the first process and the total transformation enthalpy, whereas $(1-A)$ is the ratio between enthalpy change during the second process and the total transformation enthalpy at annealing temperature T.

The data collected from the experiments are plotted and linearly-fitted according to above expressions, the value of the rate constant k can be easily obtained, which obeys the Arrhenius law:

$$k = \nu\exp\left(\frac{-E_{\mathrm{a}}}{RT}\right) \tag{5}$$

where ν is the frequency factor, and E_{a} is the apparent activation energy.

By means of above models, mullite formation kinetics of the sol–gel process was widely studied. In general, the monophasic gels (MGs) were accepted to be nucleation-controlled with an apparent activation energy (E_{a}) of 283–362 kJ mol^{-1} [10,18–20]; while diphasic gels (DGs) were dominated by a nucleation and growth mechanism in the silica-rich matrix with E_{a} of 1070–1090 kJ mol^{-1} [21,22]. However, the latest study by Tkalcec [15] showed that the apparent mullitization activation energy for MGs was similar to those of DGs, which was around 1028–1053 kJ mol^{-1}. It is interesting that various results were reported even for a so-called "atomic-or-molecular-level-mixed" alumina-silica system.

These studies are useful to clear the crystallization, transformation or mullitization reaction mechanism, but are not helpful to understand the sintering process of a mullite ceramic material, especially green compact made of kaolinite and aluminum hydroxide. The understanding and control of the sintering process, however, is very important for the appearance, microstructure and properties of mullite ceramics.

As a powerful new approach to investigate the kinetics of the sintering procedure, stepwise isothermal dilatometry (SID) was successfully used and reported by others [23–26]. Thus, it might be a solution for our research. In the kinetic study of the sintering process by dilatometry, the length shrinkage of a specimen is recorded against time. In this way, SID was used to investigate the three-dimensional isothermal sintering process. Assuming isotropic sintering, the fractional densification function Y can be expressed as:

$$Y = \frac{V_{\mathrm{o}} - V_{\mathrm{t}}}{V_{\mathrm{o}} - V_{\mathrm{f}}} = \frac{L_{\mathrm{o}}^3 - L_{\mathrm{t}}^3}{L_{\mathrm{o}}^3 - L_{\mathrm{f}}^3} \tag{6}$$

where V_{o} (L_{o}), V_{t} (L_{t}), and V_{f} (L_{f}) are the initial volume/length, volume/length at time t, and the fully-dense volume/length of the specimen respectively. A "dynamic" relative volumetric shrinkage is inferred as Makipirtti equation [23]:

$$\frac{V_{\mathrm{o}} - V_t}{V_t - V_{\mathrm{f}}} = \frac{Y}{1-Y} = [k(T)(t - t_{\mathrm{o}})]^n \tag{7}$$

where t_{o} is the beginning time of each isothermal step, and $k(T)$ is the specific rate constant which obeys the Arrhenius law. Eq. (7) has been successfully used for liquid-phase sintering of alloys [23] and solid state sintering of some metals [24].

By eliminating the $(t-t_{\mathrm{o}})$ from Eq. (7), a normalized rate equation can be developed as the Makipirtti–Meng equation [25]:

$$\frac{\mathrm{d}Y}{\mathrm{d}t} = nk(T)Y(1-Y)\left(\frac{1-Y}{Y}\right)^{\frac{1}{n}} \tag{8}$$

where n is a parameter related to the process mechanism. Eq. (8) has been employed successfully to describe the kinetics of the sintering process for Y-TZP ceramics [25] as well as pore-forming process of macroporous alumina ceramics by extrusion [26].

All of the above applications of SID are only to be used to investigate physical sintering procedure. Can it be used for a case of reactive sintering of ceramics? In this paper, we try to introduce it to the sintering kinetic study of kaolinite and aluminum hydroxide extrudate.

3. Experimental procedure

3.1. Preparation of specimens

High purity kaolinite (China Kaolinite Company), aluminum hydroxide (Shandong Aluminum Industry Company) were used and their chemical compositions are listed in Table 1. The particle size distributions of raw material powders used in this study were analyzed by Coulter LS100 (USA), and the median diameters of kaolinite and aluminum hydroxide are 12.06 and 6.14 μm while the specific surfaces of the two powders are 8019 and 10982 cm g^{-1} respectively. The mixture of kaolinite and aluminum hydroxide with 75 wt.% Al_2O_3, some pore-forming agent (e.g. carbon powder) and organic additives (e.g. cellulose derivatives) were mixed and pugged in a pug mill under vacuum to obtain a paste, the latter was then extruded into cylindrical bars through an extruder. After drying, the cylindrical green body was cut into some small pieces and small bars with dimensions of 1 × 6 × 30 mm which were used to study the sintering shrinkage process. The sintering were performed in a programmable HT furnace (Nabertherm, Germany) in air at a ramping rate of 2 °C min^{-1} up to 600 °C, followed by 5 °C min^{-1} to various temperatures (1000–1600 °C) where the specimens were soaked for 4 h and cooled naturally. The porosity of the specimens was measured according to Archimedes's method and the theoretical density of mullite-corundum ceramics was taken as 3.54 g cm^{-3} from the theoretical calculation. The average pore size and pore size distributions of the fired specimens were obtained by the bubble-point method.

3.2. Structural characterization of the specimens

XRD patterns of the sintered specimens were obtained by Kigaku D/MAz-γ_A rotating X-ray diffraction unit. The microstructure of the specimens was examined by Hitachi X-650 scanning electron microscope (Japan).

3.3. Shrinkage measurement

The sintering shrinkage measurement of the green bars was carried out by a horizontal dilatometer (Netsch type 402E, W-Germany). A special program was operated to perform a stepwise isothermal dilatometry measurement, and time (s), temperature (°C), and length shrinkage (μm) data were recorded. The SID program can be described as follows: the temperature holding steps are 900, 950, 1000, 1050, 1100, 1150, 1200, 1250, 1300, 1350, 1400 and 1450 °C for 60 min respectively, and the ramping rate between the isothermal holdings is 10.0 °C min^{-1}.

4. Results and discussion

4.1. Phase identification by X-ray diffraction

XRD results of the fired specimens (Fig. 1) reveal that after 4 h firing at 1000 °C, a big peak appears at $2\theta = 67.2°$ (0.139 nm), which agrees with the JCPDS card of γ-Al_2O_3. According to Chakravorty [27] and McConville [5], the X-ray peak intensities and lattice constants for γ-Al_2O_3 are nearly equal to those of an Al–Si spinel phase, in which some 4 coordinations of the Al ions are replaced by Si ions. Thus, the 0.139 nm peak stands for the spinel phase of not only γ-Al_2O_3 derived from dehydroxylation of aluminum hydroxide, but also the double-cation spinel from decomposition of metakaolinite.

In order to have a clear recognition, we transfer the related XRD results to Table 2. Comparing Fig. 1 with Table 2, spinel, all kinds of silica and alumina reacted and gradually formed orthorhombic mullite at above 1300 °C. The main phase above 1300 °C is orthorhombic mullite, and its relative content increased when fired at a higher temperature accompanied with a decrease of α-Al_2O_3.

4.2. Microstructure development SEM

Fig. 2 shows the fracture surface SEM photographs of specimens with different thermal histories. Organic additives had been burned out below 600 °C according to the thermal analysis. At 1000 °C, a glassy phase formed due to the release of amorphous silica and impurities in kaolinite, whose content increased when heated at 1300 °C, and then reduced at higher temperature as 1500 °C, leaving a series of pores in the material body.

4.3. Sintering shrinkage measurement

The initial length of the bar used for normal sintering shrinkage measurement was 6126 μm. The ramping rate

Table 1
Chemical compositions of the kaolinite and aluminum hydroxide (wt.%)

	SiO_2	Al_2O_3	Fe_2O_3	TiO_2	Na_2O (K_2O)	CaO	MgO	Loss on ignition
Kaolinite	45.0	35.1	1.04	0.42	0.80	0.10	0.47	−17.0
Aluminum hydroxide	0.08	64.1	0.05	–	–	–	–	34.6

from 20 to 1450 °C was constantly 2 °C min^{-1}. The plots of the length shrinkage versus temperature are shown in Fig. 3. There are about four steps before 1200 °C. The first step shrinkage appears at 200–250 °C,

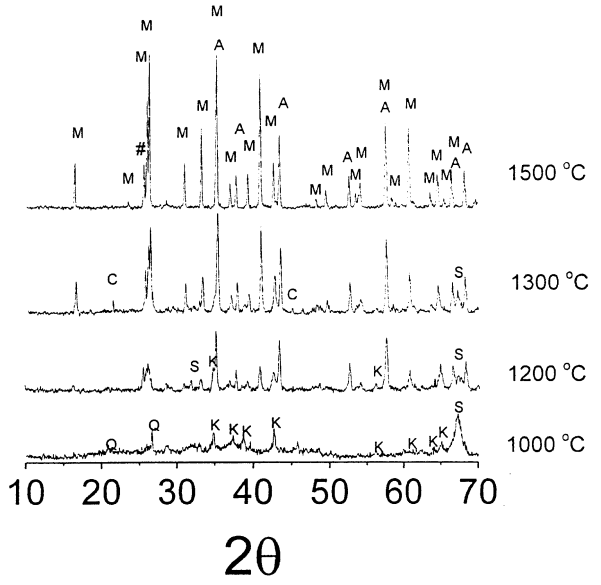

Fig. 1. The XRD patterns of the fired products of the kaolinite-aluminum hydroxide extrudate. M—Orthorhombic mullite; A—α-Al_2O_3 (corundum); C—β-SiO_2 (cristobalite); S—spinel (Al–Si spinel or γ-Al_2O_3); K—κ-Al_2O_3; Q—quartz.

Table 2
Phase compositions of the fired green body

Temperature (°C)	Main phase	Minor phase (from more to less)
1000	Spinel	κ-Al_2O_3, quartz, θ-Al_2O_3, α-SiO_2, ι-Al_2O_3, δ-Al_2O_3
1150	Mullite, spinel	κ-Al_2O_3, θ-Al_2O_3, α-SiO_2, ι-Al_2O_3
1200	α-Al_2O_3, mullite	κ-Al_2O_3, spinel, α-SiO_2
1300	Mullite, α-Al_2O_3	spinel, β-SiO_2, θ-Al_2O_3
1400	Mullite	α-Al_2O_3
1500	Mullite	α-Al_2O_3
1600	Mullite	α-Al_2O_3

where aluminum hydroxide decomposed into the alumina, releasing the structural water (according to the thermal analysis of aluminum hydroxide). The second rapid shrinkage emerges at around 400–500 °C, where the pore-forming agent and organic additives were oxidized out of the system, and kaolinite began to dehydroxylated and transformed to metakaolinite [5]. The third big shrinkage turns up at 850–950 °C, where metakaolinite was partially replaced by a spinel phase [28]. The fourth shrinkage took place at 1100–1200 °C, where some transformations took place among the different kinds of alumina (corundum is the most stable alumina and has the highest density), and a large quantity of liquid glassy phase appeared and gradually filled with the pores produced by pore-forming agent. Between 1200–1450 °C, the specimen underwent a nearly linear shrinkage with temperature.

During the steep shrinkage in the high temperature range (1200–1450 °C), the glass phase did not increase but decreased according to the SEM photographs (Fig. 2). It implies that the shrinkage might be related to the formation of mullite. However, taking the densities of corundum and glassy SiO_2 for 3.99 and 2.21 g cm^{-3} respectively, we can easily calculate that the density of their mixture with mullite component (Al_2O_3:SiO_2 = 3:2) is around 3.28 g cm^{-3}, which is slightly larger than the theoretical density of orthorhombic mullite (3.23 g cm^{-3}). Considering other kinds of silica have higher densities than glassy SiO_2, the sintering shrinkage between 1300 and 1450 °C should not attribute to mullitization reaction, though the relative peak heights of orthorhombic mullite strengthened steadily when the specimens were fired at increasing temperature (Fig. 1). On the other hand, because spinel, which still existed in the reaction system between 1200 and 1300 °C, has a lower density than corundum (for γ-Al_2O_3, $\rho = 3.62$ g cm^{-3}), the density of the mullite-component-mixture of spinel and glassy silica is around 3.06 g cm^{-3}. If the mullite is transformed or reacted from spinel, it will be possible to bring about 5.3% volume shrinkage (~1.8%

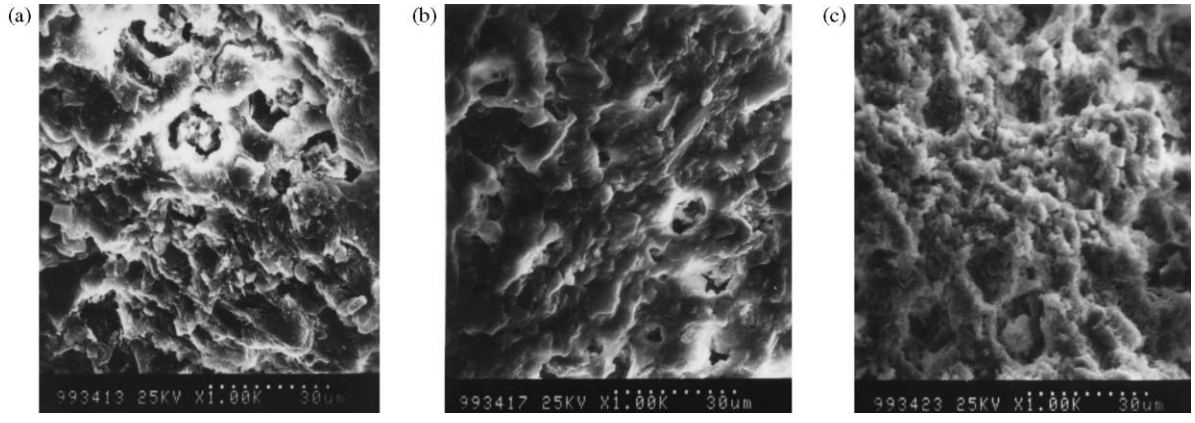

Fig. 2. The SEM photographs of the fired extrudate of the kaolinite-aluminum hydroxide: (a) 1000°C, (b) 1300°C, (c) 1500°C.

length shrinkage) during the estimated temperature range. This calculated value is slightly smaller than the real relative length shrinkage from 1200 to1300 °C in Fig. 3 (~2.2%). Therefore, mullitization reaction together with other factors affects the shrinkage during the reactive sintering.

4.4. Kinetics analysis based on SID measurement

The initial length of the green bar used for SID measurement was 6296 μm. The plots of the specimen shrinkage as well as operating temperature versus time are shown in Fig. 4.

According to Eq. (8), the related data in Fig. 4 were transferred to plots of $\ln\{(\mathrm{d}Y/\mathrm{d}t)[1/Y(1-Y)]\}$ versus $\ln[(1-Y)/Y]$ (Fig. 5) by using a computer. A very fine linear relationship is found between them for every isothermal holding, which proves that Makipirtti–Meng equation agrees with the sintering shrinkage data very well. From the slopes and intercepts of the lines, the values of exponent n and $\ln k(T)$ can be calculated and the results are listed in Table 3. In comparison with the n values in Table 3, it is obvious that there are big undulations for n between 900 and 1200 °C. Since n is a parameter related to the process, its difference reflects various sintering shrinkage mechanisms. The three biggest n values appear at 900, 1100 and 1150 °C and are pertinent to the two big shrinkages at 850–950 °C and 1100–1200 °C in Fig. 3, where spinel formed and glassy phase diffused or alumina transformed. According to the n values, the results of linear fitting can be roughly divided into three stages: (a) 1300–1450 °C, the n values are nearly equal with each other and their average value is 0.0841; (b) 1200–1300 °C, n rises with the increasing temperature and their average value is 0.0689; (c) 950–1100 °C, n rises with the increasing temperature and their average value is 0.0760.

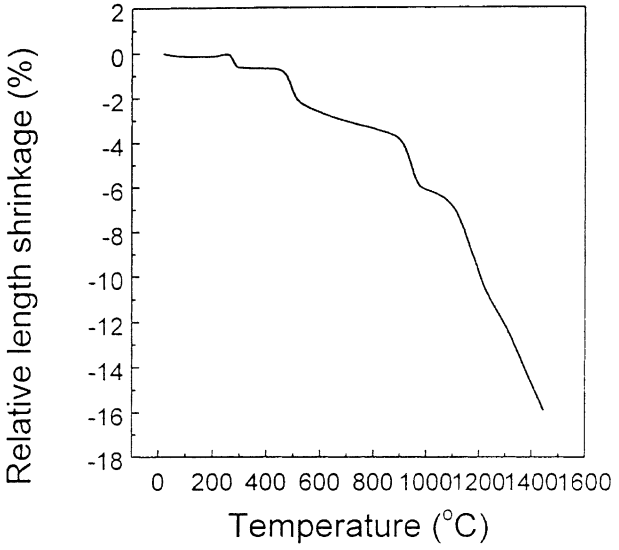

Fig. 3. The sintering length shrinkage plot of the green extrudate of the kaolinite-aluminum hydroxide.

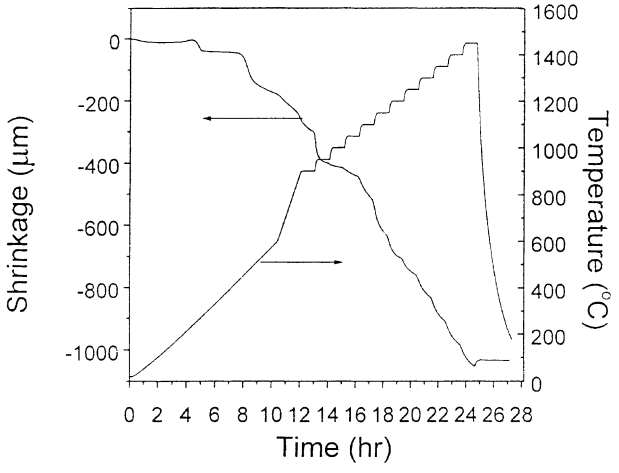

Fig. 4. The SID shrinkage curve of the green extrudate of the kaolinite-aluminum hydroxide.

The specific rate constants $k(T)$ for the sintering shrinkage are assumed to follow the Arrhenius temperature dependence [Eq.(5)], thus the apparent activation energy E_a can be derived from the slope. Fig. 6 presents plots of $\ln k(T)$ vs $1000/T$ based on the data in Table 3. The experimental results can be fitted into three straight lines according to the difference of n values. The apparent activation energies of three temperature ranges are obtained as 792.7 ± 17.0 kJ mol^{-1} for 1300–1450 °C, 1056 ± 74 kJ mol^{-1} for 1200–1300 °C, and 2972 ± 461 kJ mol^{-1} for 950–1100 °C by linear-fitting the related data.

The apparent activation energy represents energy barriers for all processes necessary for the reactive sintering of mullite-corundum ceramics. Among the calculated E_a, the value for 1200–1300 °C is in good agreement with 1034 ± 124 kJ mol^{-1} [21] and 1070 ± 200 kJ mol^{-1} [22], which refer to the apparent activation energy of mullitization in sol-gel process. Thus it suggests

Table 3
The results of linear fitting by Eq. (8)

T (°C)	$10^3/T$ (K^{-1})	Ln (nk)	$1/n$	N	Lnk	R
900	0.8524	−22.71	8.519	0.1174	−20.57	0.948
950	0.8176	−46.64	32.43	0.0308	−43.16	0.913
1000	0.7854	−40.85	27.74	0.0360	−37.53	0.373
1050	0.7558	−22.60	11.90	0.0840	−20.12	0.688
1100	0.7283	−15.30	6.531	0.1531	−13.42	0.927
1150	0.7027	−15.12	12.08	0.1015	−12.83	0.979
1200	0.6788	−17.35	9.850	0.0494	−14.34	0.982
1250	0.6565	−13.86	20.25	0.0688	−11.18	0.960
1300	0.6357	−11.30	14.54	0.0884	−8.872	0.936
1350	0.6161	−9.491	11.31	0.0851	−7.027	0.977
1400	0.5977	−7.665	11.76	0.0801	−5.140	0.976
1450	0.5803	−6.134	12.49	0.0828	−3.643	0.966

that the sintering shrinkage is dominated by mullitization reaction in the range of 1200–1300 °C (c.f. the discussions in Section 4.3). Whereas the values for other temperature ranges are either much larger or smaller than 1000 kJ mol^{-1}. Because the studied system is a porous one, into which we introduce a pore-forming agent on purpose, pore formation should be related to the sintering shrinkage. The big E_a from 950 to 1100 °C reflects the formation of glassy phase and spinel, the glassy phase and grain-boundary diffusion related to pore-formation as well as the transformation of various alumina and silica. The small E_a from 1300 to 1450 °C, however, tells mainly the diffusion related to the pore formation.

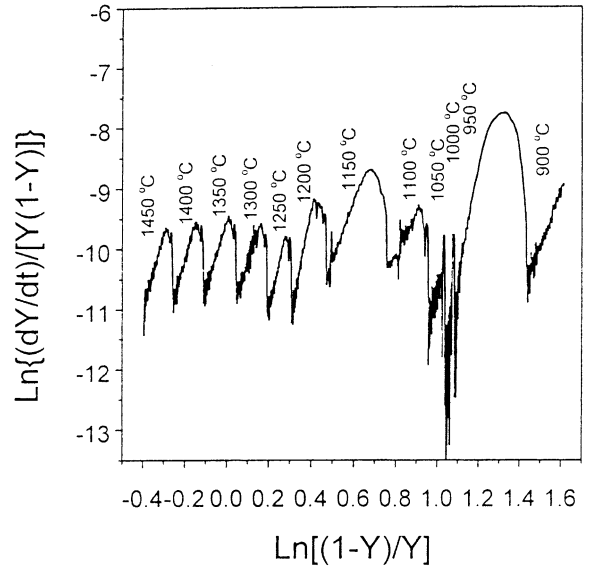

Fig. 5. Plots of $\ln\{(dY/dt)[1/Y(1-Y)]\}$ versus $\ln[(1-Y)/Y]$ according to Eq. (8).

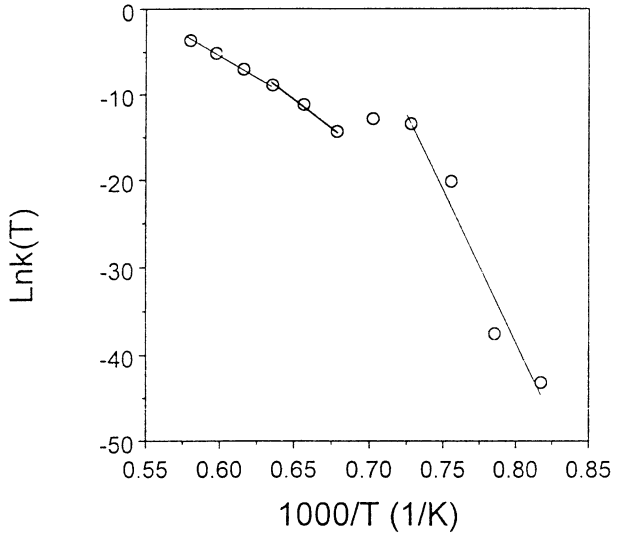

Fig. 6. Plots of $\ln k(T)$ versus $1000/T$ for the specimen.

4.5. Characterization of pore properties

The porosity of the extrudate specimens fired at various temperatures is represented in Fig. 7. The open porosity rises from 1150 to 1200 °C, then drops gradually from 1200 to 1600 °C, while the closed porosity drops at first and fluctuates with a small value later. The low open porosity at 1150 °C is due to the glassy phase, which blocked up and formed some closed pores. The total porosity keeps on decreasing at all the temperature range, agreeing with the sintering shrinkage change. The pore size distributions of specimens fired at 1300 and 1500 °C are shown in Fig. 8. The mean and maximum pore sizes are 0.521 and 0.495 μm for 1300 °C, which are smaller

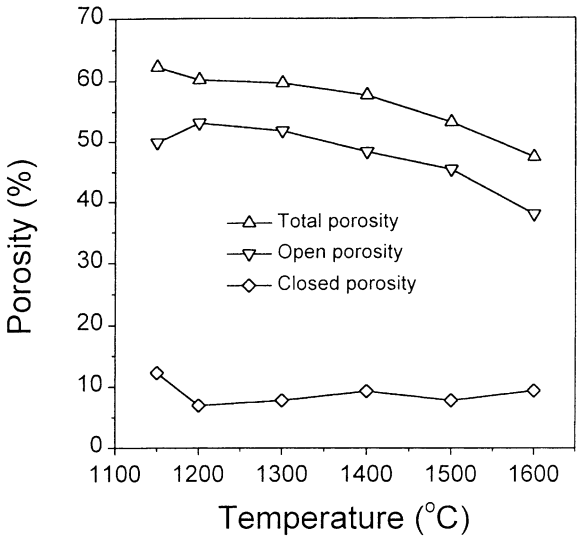

Fig. 7. The porosity of the specimens fired at different temperatures.

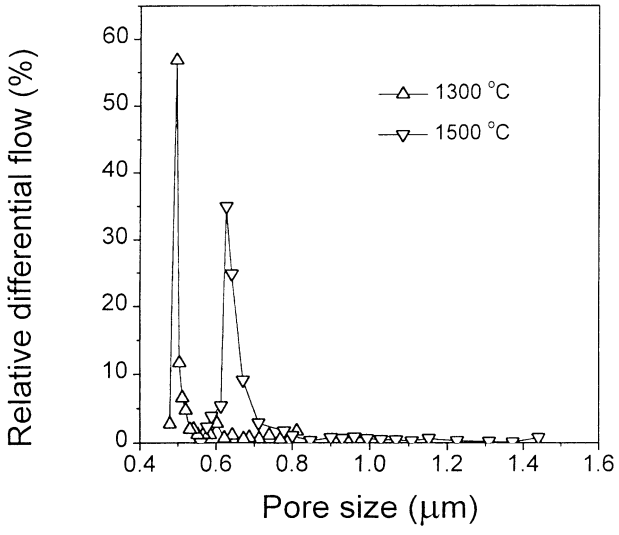

Fig. 8. The pore size distributions of the specimens fired at 1300 and 1500 °C.

than those for 1500 °C (0.675 and 0.626 μm). As a rule, the pore size should reduce when heated at a higher temperature, so it is an abnormal case in Fig. 8. As seen from the fracture photographs of SEM in Fig. 2, the glassy phase reduced from 1300 to 1500 °C. Thus the pore formation here is partly because the glassy silica diffused and reacted with corundum, forming crystalline orthorhombic mullite (c.f. Fig. 1), and partly because the small pores diffused, merged with each other, and finally disappeared. As a result, the pore formation process dominated the sintering shrinkage between 1300 and 1500 °C.

5. Conclusions

(1) The reactive sintering process for the mixture of kaolinite and aluminum hydroxide by extrusion was investigated by using XRD, SEM and stepwise isothermal dilatometry (SID) techniques, and SID data were analyzed by Makipirtti–Meng equation:

$$\frac{\mathrm{d}Y}{\mathrm{d}t} = nk(T)Y(1-Y)\left(\frac{1-Y}{Y}\right)^{\frac{1}{n}}$$

where Y is the fractional densification function.

(2) The isothermal shrinkage data agree with the Makipirtti–Meng equation very well, thus proved this equation's validity for the reactive sintering process. The shrinkage process can be divided into three stages in whole, their apparent activation energies and mean n values are obtained as 2972 ± 461 kJ mol^{-1} and 0.0760 for 950–1100 °C, 1056 ± 74 kJ mol^{-1} and 0.0689 for 1200–1300 °C, and 792.7 ± 17.0 kJ mol^{-1} and 0.0841 for 1300–1450 °C. In the first stage (950–1100 °C), the E_a based on SID is ascribed to the comprehensive effects including diffusion of glassy phase and grain-boundary, transformation of various alumina and silica, and formation of spinel. In the second stage (1200–1300 °C), E_a attributes mainly to the mullitization reaction from spinel and glassy silica. In the third stage (1300–1450 °C), E_a is dominated by the pore formation process, in which crystalline orthorhombic mullite was formed by glassy silica diffusing and reacting with corundum, and some big pores were obtained by small pores diffusing, merging and disappearing.

Acknowledgements

The authors would like to thank the Natural Science Foundation of China and Natural Science Foundation of Anhui Province for their financial supports.

References

[1] H. Schneider, E. Eberhard, Thermal expansion of mullite, J. Am. Ceram. Soc. 73 (7) (1990) 2073–2076.
[2] P. Boch, T. Chartier, Tape casting and properties of mullite and zirconia-mullite ceramics, J. Am. Ceram. Soc. 74 (10) (1991) 2448–2452.
[3] H. Schneider, M. Schmucker, et al., Optically translucent mullite ceramics, J. Am. Ceram. Soc. 76 (11) (1993) 2912–2914.
[4] I.H. Aksay, D.M. Dabbs, M. Sarikaya, Mullite for structural, electronic, and optical applications, J. Am. Ceram. Soc. 74 (10) (1991) 2343–2358.
[5] C.J. McConvile, W.E. Lee, J.H. Sharp, Microstructural evolution in fired kaolinite, Brit. Ceram. Trans. 97 (4) (1998) 162–168.
[6] I.S. Kim, Shrinkage-free mullite ceramics made from kaolin and aluminum powder, Keram Z. 45 (2) (1993) 87–90.
[7] W.A. Mariano, R.H.G.A. Kiminami, Effect of chemical composition on the sintering of mullite powders obtained by γ-Al_2O_3 and kaolin, Ceram. Trans. 51 (1995) 555–559.
[8] K.C. Liu, G. Thomas, A. Caballero, Mullite formation in kaolinite-α-alumina, Acta Metall. Mater. 42 (2) (1994) 489–495.
[9] M. Nikaido, Y. Yoshizawa, F. Saito, Effects of grinding on formation of mullite in a sintered body and its mechanical and thermal properties, J. Chem. Eng. Jpn. 29 (3) (1996) 456–463.
[10] D.X. Li, W.J. Thomson, Mullite formation kinetics of a single-phase gel, J. Am. Ceram. Soc. 73 (4) (1990) 964–969.
[11] W.J. Thomson, Dynamics X-ray diffraction: a technique for following solid-state reactions, in: W.S. Young (Ed.), Ceramic Transactions, vol. 5, Advanced Characterization Techniques for Ceramics, Am. Ceram. Soc, Westerville, OH, 1989, pp. 131–140.
[12] S.H. Hong, G.L. Messing, Mullite transformation kinetics in P_2O_5–, TiO_2–, and B_2O_3–doped aluminosilicate gels, J. Am. Ceram. Soc. 80 (6) (1997) 1551–1559.
[13] D.X. Li, W.J. Thomson, Kinetic mechanisms for mullite formation from sol–gel precursors, J. Mater. Res. 5 (9) (1990) 1963–1969.
[14] A. Gualtieri, M. Bellotto, G. Artioli, et al., Kinetic study of the kaolinite-mullite reaction sequence, part II. Mullite formation, Phy. Chem. Miner. 22 (4) (1995) 215–222.
[15] E. Tkalcec, R. Nass, J. Schmauch, et al., Crystallization kinetics of mullite from single-phase gel determined by isothermal differential scanning calorimetry, J. Non-Cryst. Solids 223 (1998) 57–72.
[16] M. Avrami, Kinetics of phase change, J. Chem. Phys. 7 (1939) 1103–1112; 8 (1940) 212–224; 9 (1991) 177–184.
[17] A. Johnson, R.F. Mehl, Reaction kinetics in processes of nucleation and growth, Trans. AIME 135 (1939) 416–442.
[18] B.E. Yoldas, D.P. Partlow, Formation of mullite and other alumina-based ceramics via hydrolytic polycondensation of alkoxides and resultant ultra- and microstructural effects, J. Mater. Sci. 23 (1988) 1895–1900.
[19] D.X. Li, W.J. Thomson, Tetragonal to orthorhombic transformation during mullite formation, J. Mater. Res. 6 (4) (1991) 819–824.
[20] J.A. Pask, A.P. Tomasia, Formation of mullite from sol–gel and kaolinite, J. Am. Ceram. Soc. 74 (10) (1991) 2367–2373.
[21] J.C. Huling, G.L. Messing, Epitactic nucleation of spinel in aluminosilicate gels and its effect on mullite crystallization, J. Am. Ceram. Soc. 74 (10) (1991) 2374–2381.
[22] W. Wei, J.W. Halloran, Transformation kinetics of diphasic aluminosilicate gels, J. Am. Ceram. Soc. 71 (7) (1988) 581–587.
[23] S. Makipirtti, in: W. Lesznski (Eds.), Powder Metallurgy, Interscience Publ., New York, London, 1961, p. 97.
[24] H. E. Exner, G. Petzow, in: G.C. Kuczynski (Eds.), Sintering Processes, Plenum Press, New York, London, 1980, pp. 107–120.
[25] G.Y. Meng, O.T. Sorensen, Kinetics analysis on low temperature sintering process for Y-TZP ceramics, in: Y. Han (Ed.), Advanced Structural Materials, vol. 2, Elsevier Science Publishers B. V, Amsterdam, Netherlands, 1991, pp. 369–374.
[26] H.T. Wang, X.Q. Liu, Kinetics and mechanism of a sintering process for macroporous alumina ceramics by extrusion, J. Am. Ceram. Soc. 81 (3) (1998) 781–784.

[27] A.K. Chakravorty, D.K. Ghosh, Crystallization behavior of Al_2O_3 in the presence of SiO_2, J. Am. Ceram. Soc. 70 (3) (1987) 46–48.

[28] G.M. Brindley, M. Nakahira, Kaolinite–mullite reaction series: I–III, J. Am. Ceram. Soc. 42 (7) (1959) 311–314; 42 (7) (1959) 314–318; 42 (7) (1959) 319–324.